The Astrophysical Journal, 596:1341–1346, 2003 October 20
© 2003. The American Astronomical Society. All rights reserved. Printed in U.S.A.

FLUX ROPE ACCELERATION AND ENHANCED MAGNETIC RECONNECTION RATE

C. Z. Cheng,[1] Y. Ren,[1] G. S. Choe,[1] and Y.-J. Moon[2,3]
Received 2003 March 6; accepted 2003 July 1

ABSTRACT

A physical mechanism of flares has emerged from our 2.5-dimensional resistive MHD simulations of the dynamical evolution of current sheet formation and magnetic reconnection and flux rope acceleration subject to the continuous, slow increase of magnetic shear in the arcade. With anomalous nonuniform resistivity in the current sheet the simulation results relate the flux rope's accelerated rising motion with an enhanced magnetic reconnection rate and thus an enhanced reconnection electric field in the current sheet during the flare rise phase. The simulation results provide good quantitative agreement with observations of the acceleration of flux ropes, which are manifested in the form of ejected soft X-ray plasmas, erupting filaments, or CMEs. For the X-class flare events studied in this paper the peak reconnection electric field is $\sim O(10^3\ \mathrm{V\ m^{-1}})$ or larger, enough to accelerate electrons to over 100 keV in a field-aligned distance of 0.1 km and produce impulsive hard X-ray emission observed during the flare rise phase.

Subject headings: methods: numerical — MHD — Sun: coronal mass ejections (CMEs) — Sun: flares

1. INTRODUCTION

Most coronal mass ejections (CMEs) are accompanied by X-ray flares, which suggests that there is a common physical mechanism underlying both phenomena (e.g., Harrison 1995; Hundhausen 1999). Recently, the cause-effect relationship between CME propagation and X-ray flare emission has been actively examined based on the combined observations of the *Solar and Heliospheric Observatory* Large Angle and Spectrometric Coronagraph Experiment (*SOHO* LASCO), the *SOHO* Michelson Doppler Imager, the *SOHO* Extreme Ultraviolet Imaging Telescope, the Big Bear Solar Observatory (BBSO) Hα, the *Transition Region and Coronal Explorer* (*TRACE*), *GOES*, the *Yohkoh* Soft X-Ray Telescope and Hard X-Ray Telescope, and the *Ramaty High Energy Solar Spectroscopic Imager* (*RHESSI*) (Alexander, Metcalf, & Nitta 2001; Neupert et al. 2001; Zhang et al. 2001; Moon et al. 2003; Gopalswamy et al. 2003; Gallagher, Lawrence, & Dennis 2003). In particular, Gallagher et al. (2003) have found that a rapid acceleration of a CME in the low corona occurs during the rise phase of the 2002 April 21 X1.5 flare. The event is first observed as a rapid rise in *GOES* X-rays, followed by simultaneous conjugate footpoint brightening and an ascending CME loop feature observed by *TRACE*. The most intense peak in hard X-ray (HXR) ($\geq$25 keV) emission observed by *RHESSI* occurs at the time of maximum acceleration of the CME upward motion. Similarly, Moon et al. (2003) have studied the relationship between CME propagation and X-ray flare emission for a set of homologous flare-CME events and found that CMEs are most accelerated in the low corona during the flare rise phase. An impulsive HXR emission was also observed during the flare rise phase. It is thus quite convincing that the CME-flare observations have established a correlation between the flare energy release and CME upward motion. The *Yohkoh* observations have also established a similar correlation between the flare energy release and the upward motion of ejected soft X-ray (SXR) plasmas, which are frequently observed above the SXR loops (Shibata et al. 1995; Ohyama & Shibata 1997, 1998). In particular, the ejected SXR plasma has two phases of rising motion: the first phase with slow rising speed coincides with the preflare phase, and the second phase with accelerated rising speed coincides with the flare impulsive phase with the HXR emission impulsively enhanced.

From these observations we note that the association of impulsive CME acceleration in the low corona with the flare rise phase is similar to the association of impulsive ejected SXR plasma acceleration with the impulsive HXR emission. Based on the sheared arcade magnetic reconnection model (Mikic, Barnes, & Schnack 1988; Forbes 1990, 1991; Sturrock 1992; Inhester, Birn, & Hesse 1992; Mikic & Linker 1994; Linker & Mikic 1995; Kusano, Suzuki, & Nishikawa 1995; Choe & Lee 1996; Amari et al. 1996; Magara, Shibata, & Yokoyama 1997; Antiochos, Devore, & Klimchuk 1999; Choe & Cheng 2000; Cheng & Choe 2001), both the coronal mass in CMEs and ejected SXR plasmas are considered to be contained in a flux rope, which contains helical field lines loosely connected to the solar surface, and the motion of CMEs and ejected SXR plasmas corresponds to the motion of the flux rope. Thus, these different physical phenomena essentially reduce to a common fundamental physical mechanism, that the impulsive flux rope acceleration is associated with the flare rise phase and the impulsive HXR emission. However, the physical mechanism governing the flare X-ray emission and the flux rope upward motion is still unresolved.

Most arcade reconnection models of flares predict that a flux rope is formed above the reconnecting current sheet by reconnection of line-tied field lines. Although the observed flare morphology (Tsuneta et al. 1992; Masuda et al. 1994) supports the arcade reconnection model in the vicinity of and under the reconnection site, the observed correlation of flux rope acceleration and flare X-ray emissions has not been explained in previous arcade reconnection models. The possibility of flux rope formation and its rising motion has indeed been confirmed by quite a few two-dimensional

[1] Princeton Plasma Physics Laboratory, Princeton University, Princeton, NJ 08543-0451; fcheng@pppl.gov.
[2] Big Bear Solar Observatory, New Jersey Institute of Technology, 40386 North Shore Lane, Big Bear City, CA 92314.
[3] Korea Astronomy Observatory, Whaam-dong, Yuseong-gu, Daejeon 305-348, Korea.

and 2.5-dimensional numerical simulations in arcade-like field geometries (Mikic et al. 1988; Forbes 1990, 1991; Inhester et al. 1992; Mikic & Linker 1994; Linker & Mikic 1995; Kusano et al. 1995; Choe & Lee 1996; Amari et al. 1996; Magara et al. 1997; Choe & Cheng 2000; Cheng & Choe 2001). However, these arcade reconnection models did not address or could not reproduce the observed relation between the flux rope acceleration and the enhanced reconnection rate. Notably, Choe & Cheng (2000, 2002) and Cheng & Choe (2001) considered a bipolar arcade as the initial condition and found a high acceleration of a flux rope due to its merging with a preexisting flux rope from above. They confirmed that the high acceleration phase coincides with the highest reconnection rate. These studies, however, adopted a uniform resistivity, and the obtained values of flux rope speed (several tens of km s^{-1}) and the acceleration and reconnection electric field ($\lesssim 10$ V m^{-1}) are relatively small compared with observations (Ohyama & Shibata 1998; Qiu et al. 2002). It is also worthwhile to point out that the flux rope model extensively tested against CME data (Chen 1989; Krall et al. 2001) is concerned with a non-MHD ejection mechanism and does not magnetic reconnection and flux rope formation processes.

In this paper, we improve our previous simulation studies (Choe & Cheng 2000, 2002; Cheng & Choe 2001) with a nonuniform anomalous resistivity model with a nonvanishing resistivity that is proportional to $(j/j_c - 1)^{\alpha}$ when the current density j is larger than a critical value j_c. For a larger α value the reconnection rate is greatly enhanced during the acceleration phase of the flux rope upward motion. For $\alpha = 2$ the simulation results can explain the observed correlation between the flux rope acceleration and enhanced magnetic reconnection rate with a quantitatively good agreement with observations during the flare rise phase. In particular, we find that the magnetic reconnection rate in the current sheet is enhanced when the flux rope upward motion is impulsively accelerated in the low corona. The acceleration of the flux rope can be further enhanced if it merges with a preexisting upper flux rope from above. The reconnection electric field, which can reach $\sim O(10^3)$ V m^{-1}, is essentially directed along the ambient magnetic field in the reconnecting current sheet and can easily accelerate electrons to an HXR-emitting energy of 100 keV in a distance of more than 0.1 km along the ambient magnetic field to produce an impulsive HXR emission during the flare rise phase.

2. FLUX ROPE ACCELERATION AND ENHANCED RECONNECTION RATE

Our model is based on resistive 2.5-dimensional MHD simulations of the evolution of a bipolar arcade (Choe & Cheng 2000; Cheng & Choe 2001). The evolution of the corona is governed by resistive MHD equations including gravity and nonuniform anomalous resistivity and assuming the plasma is isothermal. We consider the evolution of an initially closed arcade field configuration in the (x, y) plane, and the magnetic field is invariant in the z-direction. The gravity is pointing downward in the y-coordinate. The magnetic field can be expressed as $\boldsymbol{B} = \nabla\psi(x, y, t) \times \nabla_z + B_z(x, y, t)\nabla z$, where ψ is the poloidal magnetic flux. A nonuniform anomalous resistivity model is employed with $\eta = \eta_0(j_z/j_c - 1)^2$ for $j_z > j_c$ and $\eta = 0$ for $j_z \leq j_c$, $\eta_0 = 10^{-5}$, and $j_c = 1.5$. The magnetic field $\boldsymbol{B}$ is normalized by B_0, which is the maximum magnitude of the initial boundary normal field, the mass density ρ is normalized by the initial density ρ_0 at the bottom boundary, the velocity $\boldsymbol{v}$ is normalized by $V_0 = B_0/(4\pi\rho_0)^{1/2}$, the time t is normalized by $t_0 = L_0/V_0$, the current density is normalized by $j_0 = cB_0/4\pi L_0$, the electric field is normalized by $E_0 = V_0 B_0/c$, and the resistivity η is normalized by E_0/j_0, where L_0 is the length unit. A nonuniform grid is employed to resolve the current sheet structure. For typical corona parameters of $B_0 = 300$ G, electron density $n_0 = 10^9$ cm^{-3}, and $L_0 = 6 \times 10^4$ km, we have $V_0 = 2 \times 10^4$ km s^{-1}, $t_0 = 3$ s, $E_0 = 6 \times 10^5$ V m^{-1}, $j_0 = 3.98 \times 10^{-4}$ A m^{-2}, $j_c = 5.97 \times 10^{-4}$ A m^{-2}, and $E_0/j_0 = 6.5 \times 10^7$ ohm-m.

We focus on the evolution of flux ropes not totally expelled from the Sun. By imposing a shear-increasing footpoint motion with a shearing velocity $V_z(x) = V_{z0}x\exp[(1 - x^2)/2]$ and $V_{z0} = 10^{-3}V_0$, magnetic reconnection takes place to create flux ropes, and merging of flux ropes also occurs in the corona as shown in Figure 1, which shows the flux rope's O-line height versus time. There are four reconnection events in the simulation; the cross symbol in the figure indicates the formation of a new flux rope, and the circle symbol indicates the completion of the merging of two flux ropes. It is clear that each reconnection event occurs in a very short time ($10^{-3}t_0 \simeq 1$ hr for typical corona parameters) in comparison with the time interval between two successive reconnection events. Also, in the first reconnection event there is no flux rope merging involved. Note that the dynamics during the reconnection events does not depend on the shearing speed as long as it is much smaller than the Alfvén (or normalized) speed. To ensure accurate numerical results we have checked the numerical

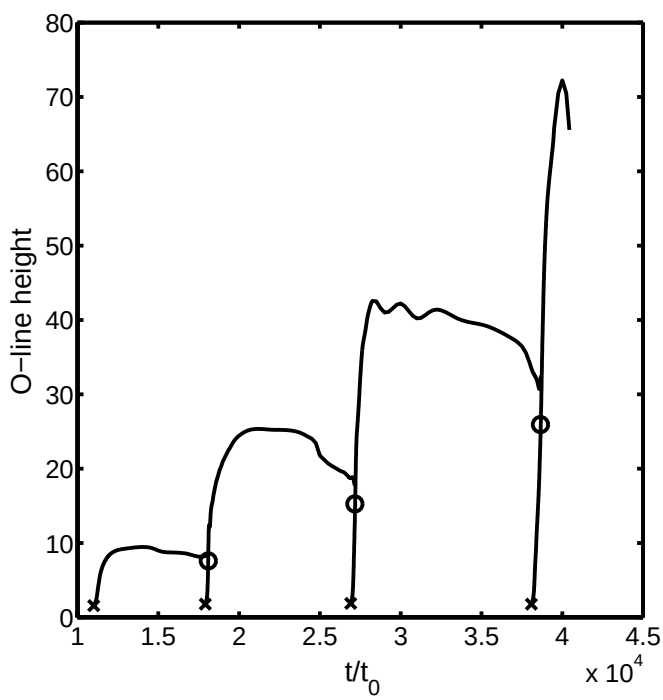

FIG. 1.—Height of O lines of the flux ropes vs. time for the MHD simulation with a nonuniform anomalous resistivity model with the resistivity parameters $\eta_0 = 10^{-5}$, $j_c = 1.5$, and the photospheric velocity shear parameter $V_{z0} = 10^{-3}V_0$. The slope of the curves represents the rising speed of the flux ropes. The cross sign indicates the formation of a new flux rope, and the circle sign indicates the completion of the merging of two flux ropes.

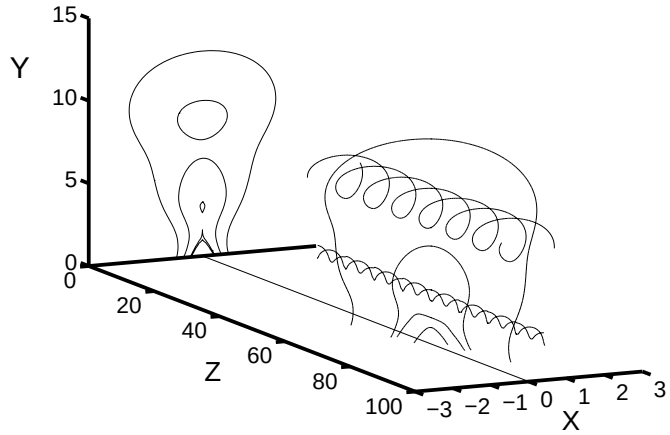

FIG. 2.—Three-dimensional magnetic field lines and their projection in the (x, y) plane at $t = 18,020t_0$ in a 2.5-dimensional MHD simulation with the maximum shearing velocity $V_{z0} = 10^{-3}V_0$ and the nonuniform resistivity parameters $\eta_0 = 10^{-5}$ and $j_c = 1.5$.

convergence over grid structure, the number of grid points, and the time step.

As the X line and the current sheet below the newborn flux rope rise, the field structure in the current sheet changes rapidly. When a flux rope is formed, the toroidal flux originally contained in the line-tied arcade is redistributed into two flux systems: the flux rope, and the underlying line-tied arcade field. The magnetic shear is thus reduced in the underlying arcade after the flux rope formation. A further increase of magnetic shear takes place in the lower arcade flux system, and above a critical value of magnetic shear magnetic reconnection causes a new flux rope to form as shown in Figure 2, which shows the three-dimensional field lines of flux ropes and closed arcade fields as well as their projection in the (x, y) plane. We note that in the flux ropes the toroidal field (B_z) is larger than the poloidal field ($B_p = |\nabla\psi|$). In the current sheet below the newborn flux rope, $B_z \gg B_p$. However, in the arcade below the current sheet, $B_z \sim B_p$. When magnetic reconnection continues, the newborn flux rope rises with an accelerated velocity and eventually merges with the overlying flux rope to form a single integrated flux rope. This process of new flux rope formation and its merging with a preexisting flux rope can be repeated as long as magnetic shear is continuously supplied.

Figure 3 shows the detailed time evolution of the flux rope's O-line height, velocity, acceleration, and magnetic reconnection rate ($\partial\psi/\partial t$, where ψ is the magnetic flux at the X line) for the four magnetic reconnection events shown in Figure 1. From Faraday's law the reconnection electric field at the X line is related to the magnetic reconnection rate by $E_z = -\partial\psi/\partial t$ in our 2.5-dimensional model. It is to be noted that although the temporal evolution of flux rope motion and reconnection rate is different for all four reconnection events, probably due to the flux rope's interaction with different surrounding fields, there are qualitative similarities. For the first three reconnection events the flux rope is first accelerated and then decelerated, while for the fourth reconnection event after the first acceleration the flux rope's velocity saturates, and then it is reaccelerated and then decelerated again. The reconnection rate increases during the first flux rope acceleration phase and then gradually decreases for a longer duration after the first flux rope acceleration subsides for all four reconnection events. Also note that the flux rope acceleration and reconnection rates are further enhanced when the magnetic merging process occurs. The reconnection electric field is peaked in the current sheet below the newborn flux rope. Moreover, because the reconnection electric field is mainly parallel to the magnetic field in the current sheet, particles can be accelerated to very high energies along the field line if the reconnection electric field is large. If we assume that the flare X-ray emission is proportional to the magnetic reconnection rate, our simulation results of flux rope acceleration and associated enhanced reconnection rate resemble the observations of flux rope acceleration in the low corona and its association with the flare rise phase and impulsive HXR emission (Ohyama & Shibata 1997, 1998; Moon et al. 2003; Gallagher et al. 2003).

From the simulation results, the phase of the newborn flux rope creation and its slow rise is regarded as the preflare phase, the accelerated newborn flux rope rise phase is interpreted as the impulsive (or rise) phase, and the phase with a longer period of decaying reconnection rate is considered as the main phase of a flare. The sequence of the above flaring events (reconnection processes) can be repeated as long as the magnetic shear is replenished, and we propose that they constitute a set of homologous flares. It is to be emphasized that the dynamics of magnetic reconnection and flux rope motion depend sensitively on the shearing velocity profile and the anomalous resistivity function, which is chosen to be $\eta_0(j/j_c - 1)^\alpha$ for $j > j_c$ and zero otherwise. For $\alpha \geq 1$ the reconnection rate and the flux rope acceleration are greatly enhanced over the results from our previous calculations, which employed a uniform resistivity ($\alpha = 0$). In § 3, we will show that for $\alpha = 2$ the simulation results of flux rope acceleration and enhanced magnetic reconnection rate (which corresponds to enhanced flare emission) agree quantitatively with observations during the flare rise phase (and impulsive hard X-ray emission).

3. COMPARISONS WITH OBSERVATIONS

Now, we make quantitative comparisons of the modeling results with observations during the X-ray flare rise phase. We first compare the third model reconnection event shown in Figure 3 with the flare-CME observations for the X1.8 X-ray flare of 2000 November 24 (Moon et al. 2003). The solid curves in the top panel of Figure 4 show the height versus time of the CME motion in the form of filament eruption in the low corona (BBSO Hα observation before 22:00 UT) and the apex of the CME frontal loop (observed by LASCO after 22:00 UT), respectively. The solid curves in the second and third panels show the corresponding velocity and acceleration, respectively, and the fourth panel shows the *GOES* X-ray emission (Moon et al. 2003). Note that an impulsive HXR emission occurs at around 21:52 UT, coinciding with the peak flux rope acceleration. It is clear that there is a correlation between the flux rope acceleration and the rise phase. To compare the simulation result with the observation, we consider a two million degree coronal background plasma, and the normalization parameters are $B_0 = 300$ G, $L_0 = 6 \times 10^4$ km, and $n_0 = 10^9$ cm^{-3}. Then, the distance between the opposite polarity magnetic patches in the coronal base is $2L_0 = 1.2 \times 10^5$ km, and the other normalized parameters are given in § 2. We plot the height, velocity, and acceleration of the flux rope O line and the reconnection rate obtained at the X line below the flux rope

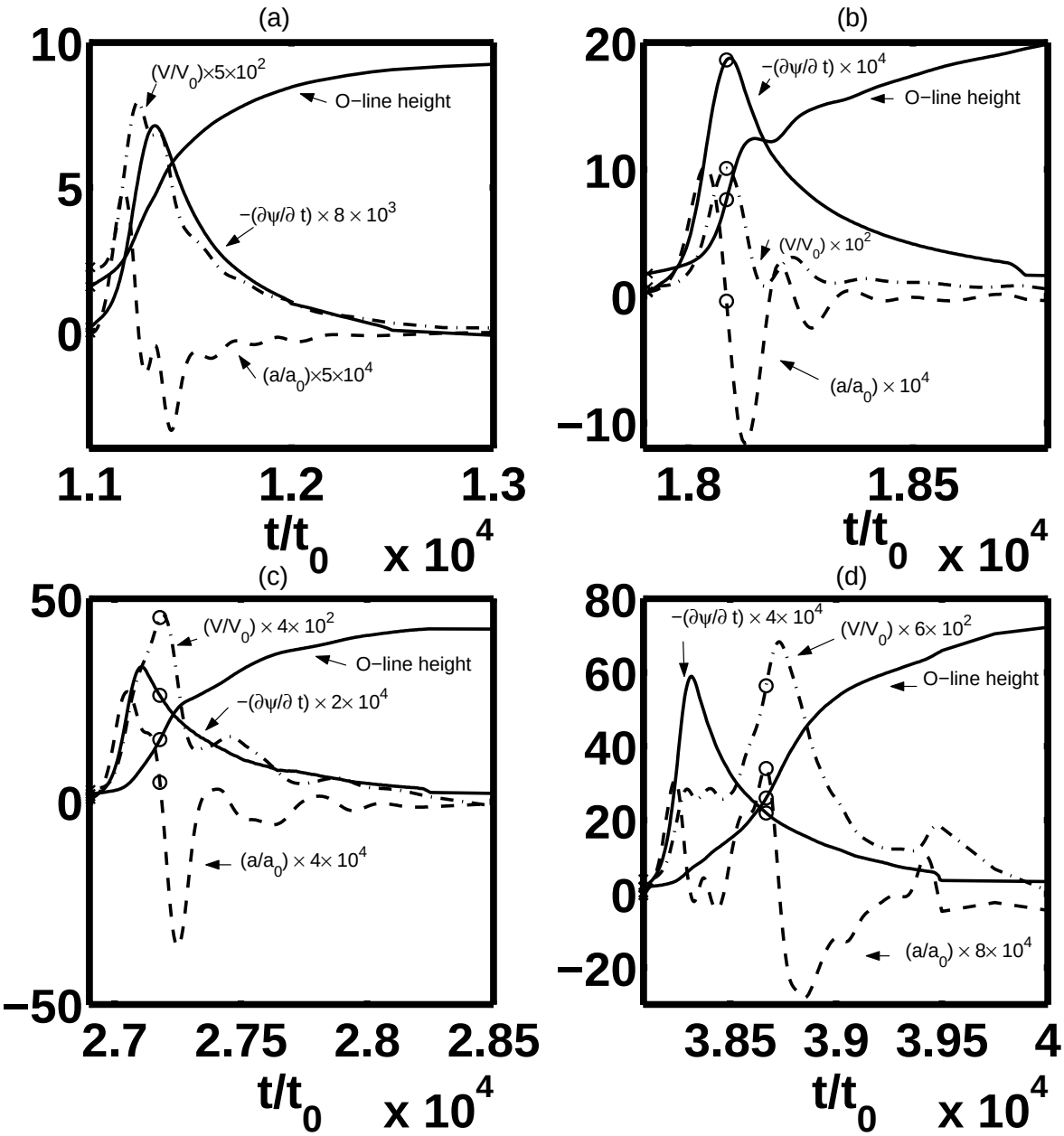

FIG. 3.—Time evolution of the flux rope's O-line height, speed, and acceleration as well as the magnetic reconnection rate in the current sheet for the four reconnection events shown in Fig. 1.

for the third simulated reconnection event shown in Figure 3*c*, and the results are shown as dotted curves in the top three panels and the bottom panel of Figure 4, respectively. The results clearly indicate that the agreement in the flux rope height, velocity, and acceleration between the observation and our model is excellent during the flux rope acceleration phase (21:45–22:00 UT). Note that the maximum reconnection rate of our model occurs almost at the same time as the observed peak CME acceleration and impulsive HXR emission, and the reconnection electric field is large with $E_{z\,\max} \simeq 1000$ V m^{-1}. With this magnetic field-aligned electric field electrons can be accelerated to $\simeq 10^3$ keV in a field-aligned distance of ≥ 1 km along the current sheet, and the acceleration distance is much smaller than the electron mean free path, which is $O(10^4)$ km for $n_e = 10^9$ cm^{-3} and $T_e = 1$ keV. For this flare event the flare rise phase lasts only about 15 minutes, and the main phase lasts about 1 hr. It is to be noted that even though the apex of the CME frontal loop surrounding the CME cavity (interpreted as the flux rope) can be as much as 30% higher than the cavity center (flux rope O line), our conclusion remains intact. Thus, if the height data of the CME cavity center from LASCO is used, the differences in the height, velocity, and acceleration during the flare main phase should be much reduced. Another factor responsible for the differences in the height, velocity, and acceleration during the flare main phase in the comparison could be due to different surrounding field in the simulation from the actual coronal field. These issues will be addressed in the future studies. Finally, a comparison has also been made with the 2002 April 21 X1.5

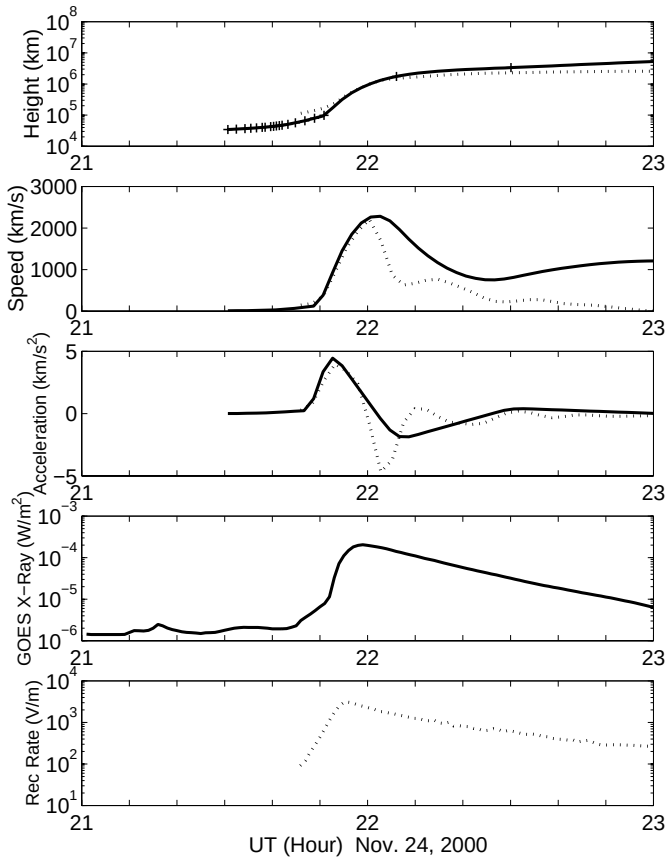

FIG. 4.—Solid curves in the top four panels show the time evolution of height (relative to the solar limb), speed, and acceleration of the filament eruption in the low corona and CME in the higher corona associated with a 2000 November 24 X1.8 flare and the corresponding *GOES* X-ray flux, respectively. The impulsive HXR emission occurs around 21:52 UT, which coincides with the peak CME acceleration. The dotted curves in the top three panels and the bottom panel shows the model results of flux rope height, speed, acceleration, and reconnection rate (or reconnection electric field) for the third reconnection event shown in Fig. 3*c*.

flare-CME event presented by Gallagher et al. (2003), and a similar agreement was obtained during the flare rise (and flux rope acceleration) phase.

Next, we compare the first model reconnection event shown in Figure 3 with the *Yohkoh* observation of the 1993 November 11 C9.7 flare that showed an acceleration of an ejected SXR plasma and associated impulsive HXR emission as shown in Figure 3 of Ohyama & Shibata (1997). For this flare event the ejected SXR plasma rises to a height of $\simeq 2.6 \times 10^4$ km with a velocity of $\simeq 60$ km s^{-1} at 11:16 UT, to $\simeq 3 \times 10^4$ km with a velocity of $\simeq 110$ km s^{-1} at 11:17 UT, to $\simeq 3.8 \times 10^4$ km with a velocity of $\simeq 140$ km s^{-1} at 11:18 UT, to $\simeq 4.9 \times 10^4$ km with a velocity of $\simeq 160$ km s^{-1} at 11:19 UT, to $\simeq 5.8 \times 10^4$ km with a velocity of $\simeq 180$ km s^{-1} at 11:20 UT, and then rises almost linearly to $\simeq 9 \times 10^4$ km with a velocity of $\simeq 200$ km s^{-1} at 11:23 UT. Thus, there is an ejected SXR plasma acceleration phase during 11:16–11:23 UT. The maximum acceleration occurs at about 11:17:30 UT. The HXR emission in the 14–23 keV HXT energy band is enhanced during 11:15–11:26 UT, and emission for the 23–33 keV HXT energy band is enhanced during 11:15–11:18 UT. To compare the first reconnection event shown in Figure 3*a* with this *Yohkoh* event, we choose the normalization quantities to be $B_0 = 200$ G, $n_0 = 10^9$ cm^{-3}, and $L_0 = 2.2 \times 10^4$ km. Then, $V_0 = 1.3 \times 10^4$ km s^{-1}, $t_0 = 1.7$ s, the acceleration normalization $a_0 = V_0/t_0 = 7.6 \times 10^3$ km s^{-2}, and $E_0 = 2.6 \times 10^4$ V m^{-1}. If we assume that the flux rope begins to be accelerated at 11:16 UT, the maximum velocity reaches $V_{\max} \simeq 210$ km s^{-1} at the flux rope height of 8.4×10^4 km at about 11:23 UT. The maximum acceleration $a_{\max} \simeq 0.73$ km s^{-2} occurs at the flux rope height of 5×10^4 km at about 11:20 UT. At the maximum reconnection rate the maximum reconnection electric field is $E_{z\max} \simeq 23$ V m^{-1} at about 11:26 UT. These model numbers are in reasonably good agreement with the observations.

It is to be noted that the 2000 November 24 X1.8 X-ray flare event is well fitted with the third reconnection event in the simulation, and the 1993 November 11 C9.7 flare is well fitted with the first reconnection event in the simulation. These two reconnection events have different dynamics of flux rope motion and reconnection rates as shown in Figure 3 because the surrounding field is different. Therefore, this result indicates that the flux rope motion is controlled by its surrounding field as well as the resistivity model in the current sheet.

These two encouraging quantitative comparisons between our modeling results and observations strongly suggest that the magnetic reconnection model can account for the observed flux rope acceleration and flare rise phase because the reconnection rate is impulsively enhanced during the flux rope acceleration, and the enhanced reconnection electric field is large enough to accelerate particles to high energies. On the other hand, we emphasize that the simulated flux rope motion is only compared with observations in the low corona because our simulations do not address the escape of flux rope from the Sun as in the CME observation. In our simulation, the flux rope speed decreases as the reconnection rate decreases. The issue of flux rope escape would require the flux rope to break through the overlying fields possibly by the expansion of the overlying fields and continuing magnetic reconnection below the flux rope, which is beyond the scope of the present study.

4. SUMMARY AND DISCUSSION

A physical mechanism of flares, in particular, for the flare rise phase, has emerged from our 2.5-dimensional MHD simulations with gravity and nonuniform anomalous resistivity. The simulation results are very encouraging because they directly relate the flux rope's accelerated rising motion with an enhanced magnetic reconnection rate and thus an enhanced reconnection electric field in the current sheet during the flare rise phase. Moreover, the peak reconnection electric field is $\sim O(10^3)$ V m^{-1} or larger, enough to accelerate particles to 100 keV in a field-aligned distance of 0.1 km. Nonthermal electrons thus generated can produce HXRs, consistent with impulsive HXR emission observed during the flare rise phase. It should be emphasized that our simulation results are the first to provide a good agreement with observations of the acceleration of flux ropes, which are manifested in the form of ejected SXR plasmas or erupting filaments or CMEs, in the low corona during the flare rise phase.

Although the flux rope is generated by reconnection of line-tied fields in the current sheet via footpoint shearing motion in our model, the correlation between the flux rope

acceleration and the reconnection rate does not depend on this specific flux rope generation process. Moreover, observations also show that there are other possibilities of creating sheared magnetic fields in the arcade for current sheet formation and allowing flux rope to be generated via reconnection. Thus, we need to extend this work in the future by investigating other methods of generating flux ropes. First, flux ropes may be generated below the solar surface and emerge in the corona, and once the rising motion of the flux rope sets in (e.g., Chen 1989; Forbes 1990), current sheet thinning and magnetic reconnection can be induced below the flux rope in the line-tied field wrapping the flux rope. Second, the magnetic shear increase need not be due to footpoint motions but can also due to the emergence of presheared magnetic flux into the corona as suggested by observations (e.g., Kundu, Woodgate, & Schmahl 1989; Kurokawa 1989). Additionally, we need to improve our simulation model to three-dimensional geometries and with a spherical boundary as in the real Sun. The flux rope dynamics in the upper corona in three-dimensional geometries can be significantly different from the 2.5-dimensional cases, and three-dimensional simulations will provide more realistic assessment of the flux rope dynamics and its relation with the flare energy release.

This work was supported by the DOE Contract DE-AC02-76-CHO3073. Y.-J. M. is supported by a MURI grant of AFOSR and by National Research Lab. M10104000059-01J000002500 of the Korean government.

REFERENCES

Alexander, D., Metcalf, T. R., & Nitta, N. 2001, Geophys. Res. Lett., 29, 41-1
Amari, T., Luciani, J. F., Aly, J. J., & Tagger, M. 1996, A&A, 306, 913
Antiochos, S. K., Devore, C. R., & Klimchuk, J. A. 1999, ApJ, 510, 485
Chen, J. 1989, ApJ, 338, 453
Cheng, C. Z., & Choe, G. S. 2001, Earth Planets Space, 53, 597
Choe, G. S., & Cheng, C. Z. 2000, ApJ, 541, 449
———. 2002, Phys. Plasmas, 9, 2330
Choe, G. S., & Lee, L. C. 1996, ApJ, 472, 372
Forbes, T. G. 1990, J. Geophys. Res., 95, 11919
———. 1991, Geophys. Astrophys. Fluid Dyn., 62, 16
Gallagher, P. T., Lawrence, G. R., & Dennis, B. R. 2003, ApJ, 588, L53
Gopalswamy, N., Shimojo, M., Lu, W., Yashiro, S., Shibasaki, K., & Howard, R. A. 2003, ApJ, 586, 562
Harrison, R. A. 1995, A&A, 304, 585
Hundhausen, A. J. 1999, in The Many Faces of the Sun, ed. K. T. Strong, J. L. R. Saba, B. M. Haisch, & J. T. Schmelz (New York: Springer), 143
Inhester, B., Birn, J., & Hesse, M. 1992, Sol. Phys., 138, 257
Krall, J., Chen, J., Duffin, R. T., Howard, R. A., & Thompson, B. J. 2001, ApJ, 562, 1045
Kundu, M., Woodgate, B. E., & Schmahl, E. J., eds. 1989, Energetic Phenomena on the Sun (Dordrecht: Kluwer)
Kurokawa, H. 1989, Space Sci. Rev., 51, 49
Kusano, K., Suzuki, Y., & Nishikawa, K. 1995, ApJ, 441, 942
Linker, J. A., & Mikic, Z. 1995, ApJ, 438, L45
Magara, T., Shibata, K., & Yokoyama, T. 1997, ApJ, 487, 437
Masuda, S., Kosugi, T., Hara, H., Tsuneta, S., & Ogawara, Y. 1994, Nature, 371, 495
Mikic, Z., Barnes, D. C., & Schnack, D. D. 1988, ApJ, 328, 830
Mikic, Z., & Linker, J. A. 1994, ApJ, 430, 898
Moon, Y.-J., Moon, Y. J., Choe, G. S., Wang, H., Park, Y. D., & Cheng, C. Z. 2003, Big Bear Solar Obs. Rep. BBSO-1173, 2003
Neupert, W. M., Thompson, B. J., Gurman, J. B., & Plunkett, S. P. 2001, J. Geophys. Res., 106, 25215
Ohyama, M., & Shibata, K. 1997, PASJ, 49, 249
———. 1998, ApJ, 499, 934
Qiu, J., Lee, J., Gary, D. E., & Wang, H. 2002, ApJ, 565, 1335
Shibata, K., Masuda, S., Hara, H., Yokoyama, T., Tsuneta, S., Kosugi, T., & Ogwara, Y. 1995, ApJ, 451, L83
Sturrock, P. A. 1992, in IAU Colloq. 133, Eruptive Solar Flares, ed. Z. Švestka, B. V. Jackson, & M. E. Machado (Berlin: Springer), 397
Tsuneta, S., Hara, H., Shimizu, T., Acton, L. A., Strong, K. T., Hudson, H. S., & Ogawara, Y. 1992, PASJ, 44, L63
Zhang, J., Dere, K. P., Howard, R. A., Kundu, M. R., & White, S. M. 2001, ApJ, 559, 452